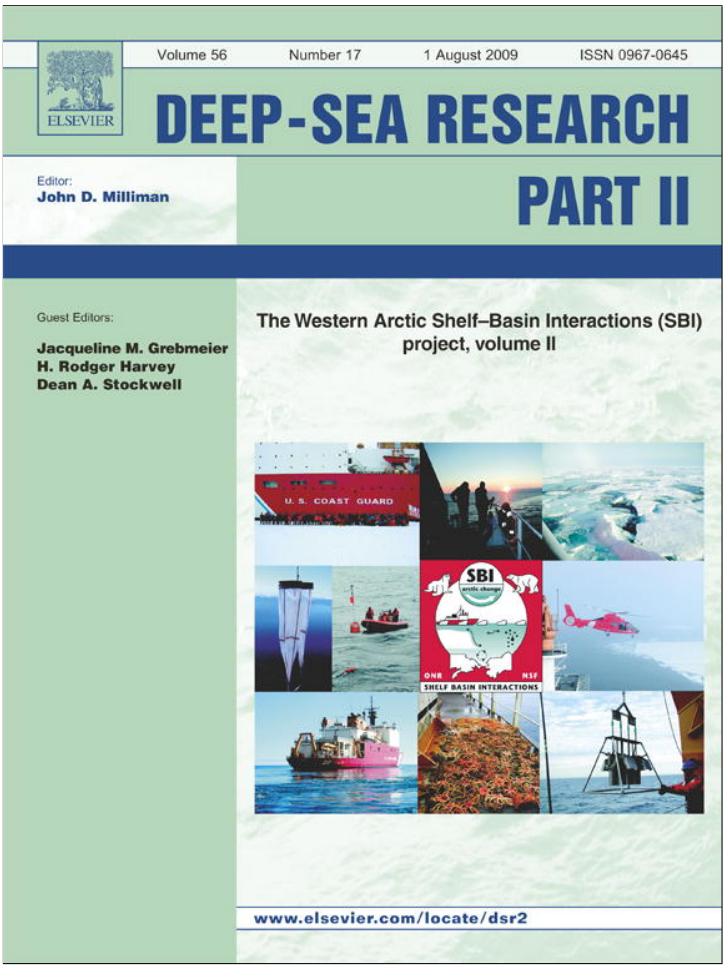

Deep-Sea Research II 56 (2009) 1351–1362

Contents lists available at ScienceDirect

Deep-Sea Research II

journal homepage: www.elsevier.com/locate/dsr2

On the processes controlling shelf–basin exchange and outer shelf dynamics in the Bering Sea

J. Clement Kinney [a,*], W. Maslowski [a], S. Okkonen [b]

[a] Department of Oceanography, Naval Postgraduate School, Monterey, CA 93943, USA
[b] Institute of Marine Science, University of Alaska, Fairbanks, AK 99775-7220, USA

ARTICLE INFO

Article history:
Accepted 31 October 2008
Available online 11 November 2008

Keywords:
Bering Sea
Polar oceanography
Numerical models
Ocean circulation

ABSTRACT

We use a 9-km pan-Arctic ice–ocean model to better understand the circulation and exchanges in the Bering Sea, particularly near the shelf break. This region has, historically, been undersampled for physical, chemical, and biological properties. Very little is known about how water from the deep basin reaches the large, shallow Bering Sea shelf. To address this, we examine here the relationship between the Bering Slope Current and exchange across the shelf break and resulting mass and property fluxes onto the shelf. This understanding is critical to gain insight into the effects that the Bering Sea has on the Arctic Ocean, especially in regard to recent indications of a warming climate in this region. The Bering Sea shelf break region is characterized by the northwestward-flowing Bering Slope Current. Previously, it was thought that once this current neared the Siberian coast, a portion of it made a sharp turn northward and encircled the Gulf of Anadyr in an anticyclonic fashion. Our model results indicate a significantly different circulation scheme whereby water from the deep basin is periodically moved northward onto the shelf by mesoscale processes along the shelf break. Canyons along the shelf break appear to be more prone to eddy activity and, therefore, are associated with higher rates of on-shelf transport. The horizontal resolution configured in this model now allows for the representation of eddies with diameters greater than 36 km; however, we are unable to resolve the smaller eddies.

Published by Elsevier Ltd.

1. Introduction

The Bering Sea is a high-latitude, semi-enclosed sea with an extensive (>500 km) continental shelf in the east and a narrow continental shelf to the west (<100 km). Portions of the shelf and coastal region experience seasonal sea-ice cover for approximately 7 months per year, with ice reaching the shelf break in the late winter of some years. The Bering Sea, like many subpolar seas, is characterized by seasonal extremes between winter and summer temperatures. Because this region is an important national and international fishery, much fisheries research has been conducted in some parts of the Bering Sea (e.g., Busby et al., 2005; Ciannelli and Bailey, 2005; Mueter et al., 2006). However, relatively little work has been done in other marine science fields, particularly in numerical modeling.

The research presented here builds on an earlier work (Clement et al., 2005), which utilized results from the same model to quantify the volume and property fluxes through the straits of the northern Bering Sea. The current work seeks to identify and discuss the regions and processes of shelf–basin exchange within the Bering Sea. It is also an attempt to provide a quantitative measure of mean volume and property fluxes across the outer shelf, defined as a region between 50- and 200-m isobaths. This exchange is important for biological productivity along the slope and on the Bering Sea shelf because the deep Bering Sea basin is the main source of nutrients for these locations. In addition, the biological production within the Chukchi and Beaufort Seas is strongly dependent on the influx of nutrients from the deep Bering Sea via Bering Strait (Codispoti et al., 2005). Without this nutrient source, biological production on the Bering Sea shelf and, consequently, in the Western Arctic would be much lower.

2. Model description

The coupled sea-ice–ocean model has a horizontal grid spacing of 1/12° (or ~9 km), and 45 vertical depth layers with eight levels in the upper 50 m and 15 levels in the upper 200 m. The high vertical resolution, especially in the upper water column, allows for more realistic representation of the shallow Arctic and sub-Arctic shelves. Some previous models of the Bering Sea were two-dimensional (e.g., Overland and Roach, 1987; Spaulding et al., 1987), which restricted their ability to represent shelf–basin

* Corresponding author.
E-mail address: jlclemen@nps.edu (J. Clement Kinney).

0967-0645/$ - see front matter Published by Elsevier Ltd.
doi:10.1016/j.dsr2.2008.10.023

exchange. More recent work in the Bering Sea includes that of Overland et al. (1994). They used a primitive equation, three-layer hydrodynamic model at 1/8° horizontal resolution. However, the domain did not include the shelf and slope, but was instead limited to the Bering Sea basin only. Mizobata et al. (2006) use a numerical model based on the Princeton Ocean Model (POM; Blumberg and Mellor, 1987) to simulate the eddy field in the vicinity of Zhemchug Canyon. While this model has a high horizontal resolution (5 km), the domain covers only a fraction of the Bering Sea slope and results may be significantly influenced by the prescribed lateral boundary forcing. The following analyses presented in this paper cover the entire deep basin, slope, and shelf of the Bering Sea, by use of the pan-Arctic domain as discussed below.

The horizontal grid in our new model permits calculation of flow through the narrow straits of the northern and southern Bering Sea. The 9-km horizontal resolution allows us to minimally resolve eddies with diameters as small as 36 km; however, we probably cannot resolve the smallest eddies. The Bering Sea has a Rossby radius of deformation of ~12–20 km according to Chelton et al. (1998). The model domain contains the sub-Arctic North Pacific (including the Sea of Japan and the Sea of Okhotsk) and North Atlantic Oceans, the Arctic Ocean, the Canadian Arctic Archipelago (CAA), and the Nordic Seas (see Fig. 1A of Maslowski et al., 2004 or www.oc.nps.navy.mil/NAME/name.html for model domain). The region of interest, the Bering Sea, is therefore far away from the artificially closed lateral boundaries in the North Pacific at 30°N, greatly reducing the potential effect of boundary conditions. Model bathymetry is derived from two sources: ETOPO5 at 5-min resolution for the region south of 64°N and International Bathymetric Chart of the Arctic Ocean (IBCAO; Jakobsson et al., 2000) at 2.5-km resolution for the region north of 64°N. The ocean model was initialized with climatological, three-dimensional temperature and salinity fields (Polar Science Center Hydrographic Climatology; PHC; Steele et al., 2000) and integrated for 48 years in a spin-up mode. During the spinup we initially used daily averaged annual climatological atmospheric forcing derived from 1979 to 1993 reanalysis from the European Centre for Medium-Range Weather Forecasts (ECMWF) for 27 years. We then continued the spinup using repeated 1979 ECMWF annual cycle for 6 years and then 1979–1981 interannual fields for the last 15 years of spinup. This approach is especially important in establishing realistic ocean circulation representative of the time period at the beginning of the actual interannual integration. At the same time, the spin-up procedure was designed to force the model into a quasi-equilibrium state that is minimally sensitive to the specific initial conditions. The final run with realistic daily averaged ECMWF interannual forcing starts in 1979 and continues through 2004. Results from this integration (26 years) are used for the analyses in this paper. Yukon (and other Arctic) river runoff is included in the model as a virtual freshwater flux at the river mouth. However, in the Gulf of Alaska the freshwater flux from runoff (Royer, 1981) is introduced by restoring the surface ocean level (of 5 m) to climatological (PHC) monthly mean temperature and salinity values over a monthly time scale (as a correction term to the explicitly calculated fluxes between the ocean and overlying atmosphere or sea ice). This approach was used due to the lack of realistic discharge observations for the many small rivers that empty into the Gulf of Alaska. Additional details on the model including sea ice, river runoff, and restoring have been provided elsewhere (Maslowski and Lipscomb, 2003; Maslowski et al., 2004).

3. General circulation

Twenty-six-year (1979–2004) mean (0–6250 m) modeled circulation and total kinetic energy (TKE) are shown in Fig. 1. TKE is calculated as $(u^2+v^2)/2$, with u and v representing the x- and y-components of velocity. TKE is useful for determining

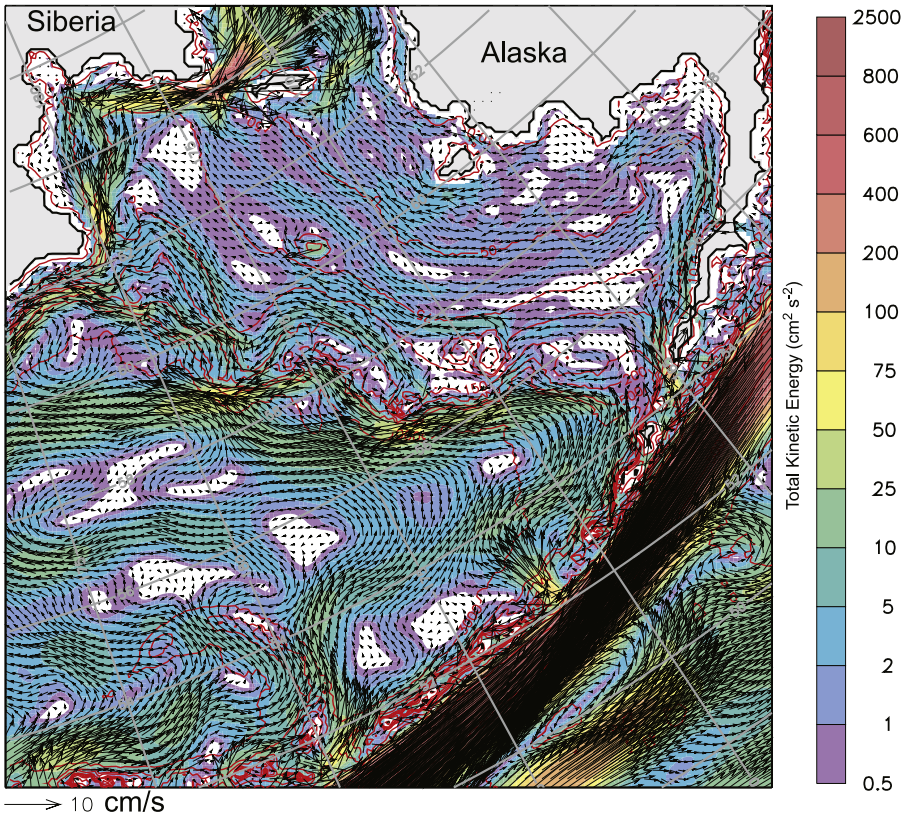

Fig. 1. Twenty-six-year (1979–2004) mean 0–220 m circulation and total kinetic energy. Every second vector is shown.

the relative speed of a current. The Alaskan Stream to the south of the Aleutian Island Chain and Anadyr Current (between Siberia and St. Lawrence Island) reach mean speeds in excess of 35 cm/s. The Bering Slope Current (BSC) is characterized by speeds up to ~12 cm/s in the long-term mean. The Bering Sea middle shelf domain ranges between <1 and 7 cm/s, with higher speeds located north of the Zhemchug Canyon region (~170–175°W).

Previous modeling and observational studies (Kinder et al., 1986, see Fig. 5; Walsh et al., 1989; Shuert and Walsh, 1993) mention that the BSC splits into two branches as it nears the coast of Siberia near Cape Navarin. One branch was believed to turn north and circulate around the Gulf of Anadyr, while the other was thought to turn southward and eventually, form part of the Kamchatka Current. However, little direct observational evidence is available to substantiate this idea. Our model results show that the vast majority of the BSC follows the bathymetry and turns south as it nears Cape Navarin (Fig. 1). Very little to none of the water from the BSC turns northward on nearing the Siberian coast. There is also evidence of a narrow coastal current flowing northward around the cape. However, this northward flowing water is not derived from BSC water. Instead, it is part of the Kamchatka Current, originating in the southern Bering Sea (not shown). Based on their observations, Stabeno et al. (1999) propose a schematic circulation in agreement with our results showing the majority of BSC water turning southward near Cape Navarin.

In an effort to visually simplify the mean circulation, we have constructed a schematic circulation based on Fig. 1, which is shown in Fig. 2. This is an update to a previously published schematic (Fig. 1 in Clement et al., 2005) and the major difference is the above-mentioned southward turn of the BSC as opposed to a north–south split. The current schematic shows the generally northwestward flow across the shelf, as well as the Anadyr Current and Alaska Coastal Current (ACC). The Alaskan Stream is the strongest with significant throughflow (primarily northward into the Bering Sea) occurring through Unimak Pass and Amukta Pass.

4. Volume transport

We have created a series of cross-sections that approximates the 50- and 200-m isobaths and several sections connecting the two isobaths. Monthly mean values of volume, heat, salt, and freshwater flux across each section were calculated for the years 1979–2004. Table 1 shows the 26-year mean values of these fluxes for each cross-section. The section locations are shown and labeled in Fig. 2. Fig. 3A shows the 26-year mean value of volume transport (Sv) across each section with an arrow indicating the mean direction of flow. Arrows are scaled as a percentage of the largest cross-sectional value shown in the figure (e.g., a volume transport of 0.5 Sv would have an arrow twice as wide as a section with volume transport of 0.25 Sv). The net volume transport is positive (on-shelf) in the central and eastern part of the Bering Sea along the 200-m isobath. It is highest through the section north of Unimak Pass (AS1). In contrast, the westernmost sections (AS7–AS9) have relatively small negative (off-shelf) mean volume transport values. This is largely due to the separation of the BSC from the shelf break west of AS6, which removes the source of large (>0.05 Sv) on-shelf transports. The cross-shelf sections (CS1–CS6) increase in volume transport from east to west, as upwelled water is accumulated and integrated into a generally northwestward flow along the outer shelf. The sharpest increase between consecutive cross-shelf sections occurs between CS3 and CS4 (increase of 0.224 Sv) over a distance of approximately 230 km. This increase in shelf transport is due to water being moved on-shelf through the Zhemchug Canyon (AS4–AS6) to the south. Sections along the 50-m isobath have very small values of

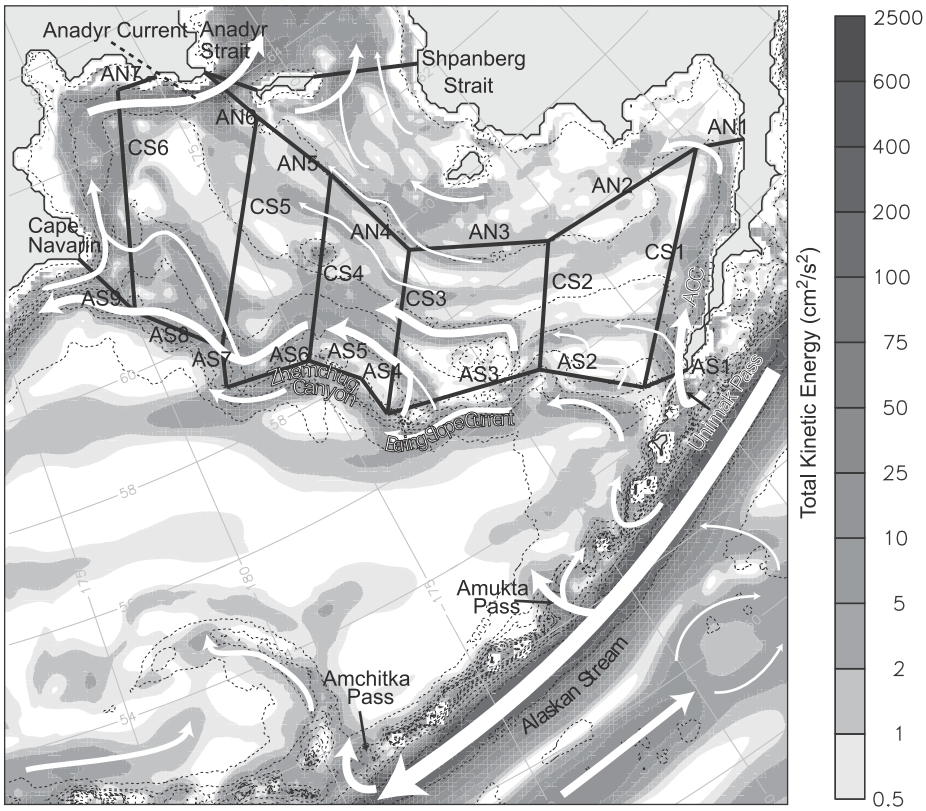

Fig. 2. Schematic circulation (0–220 m) and total kinetic energy based on Fig. 1. The locations of model cross-sections and names are included.

net volume transport, except for section AN6, which has a value of 0.528 Sv or ~83% of the total net northward volume transport across the 50-m isobath. Bathymetric steering is the main cause of the low volume transports through sections AN1–AN5, since the 50-m isobath directs water toward AN6 and eventually through Anadyr Strait, which is a deeper pass than the eastern Shpanberg Strait.

Table 1
Twenty-six-year mean volume transport (Sv), salt flux (million kg/s), freshwater flux (mSv; relative to 34.8), and heat transport (TW; relative to −0.1 °C).

Section	Volume transport	Salt flux	Freshwater flux	Heat flux
AS1	0.200 (0.097)	6.398 (3.095)	16.142 (7.992)	5.052 (2.909)
AS2	0.142 (0.092)	4.562 (2.961)	10.803 (7.128)	2.951 (2.165)
AS3	0.145 (0.146)	4.687 (4.686)	10.669 (10.867)	2.351 (2.984)
AS4	0.093 (0.063)	2.991 (2.042)	6.701 (4.599)	1.755 (1.315)
AS5	0.124 (0.070)	4.021 (2.279)	8.877 (5.001)	2.184 (1.485)
AS6	0.125 (0.137)	4.052 (4.433)	8.435 (9.435)	2.164 (2.448)
AS7	−0.086 (0.103)	−2.777 (3.345)	5.897 (7.063)	−1.189 (1.891)
AS8	−0.003 (0.100)	−0.111 (3.223)	−0.146 (7.086)	0.555 (1.476)
AS9	−0.048 (0.316)	−1.545 (10.179)	−3.360 (23.526)	0.192 (2.459)
CS1	0.168 (0.146)	5.367 (4.654)	13.875 (12.092)	2.438 (3.797)
CS2	0.280 (0.152)	8.950 (4.854)	22.939 (12.246)	3.372 (2.487)
CS3	0.355 (0.276)	11.383 (8.849)	28.004 (21.438)	3.808 (28.004)
CS4	0.579 (0.297)	18.602 (9.541)	44.927 (22.971)	5.184 (3.778)
CS5	0.606 (0.333)	19.483 (10.712)	46.523 (25.698)	4.252 (3.507)
CS6	0.073 (0.312)	2.331 (10.013)	6.158 (24.108)	0.895 (2.380)
AN1	0.042 (0.049)	1.336 (1.559)	3.732 (4.453)	1.506 (1.835)
AN2	0.023 (0.089)	0.718 (2.814)	2.101 (8.439)	0.061 (1.951)
AN3	0.067 (0.122)	2.118 (3.848)	6.037 (11.000)	0.536 (1.533)
AN4	−0.017 (0.074)	−0.526 (2.347)	−1.445 (6.721)	0.027 (1.171)
AN5	0.011 (0.080)	0.361 (2.568)	0.786 (6.656)	0.067 (0.816)
AN6	0.528 (0.187)	17.065 (5.973)	37.644 (16.393)	1.737 (2.533)
AN7	−0.019 (0.018)	−0.620 (0.581)	−1.058 (1.066)	−0.042 (0.130)
Shpanberg Strait	0.132 (0.128)	4.219 (4.040)	10.607 (11.793)	1.058 (2.187)
Anadyr Strait	0.521 (0.179)	16.842 (5.700)	37.247 (16.173)	1.799 (2.597)

Numbers in parenthesis represent standard deviation.

5. Heat transport

We calculated the heat flux referenced to −0.1 °C through the sections shown in Fig. 2. Pathways of heat transport onto and across the Bering Sea shelf are somewhat different than those of volume transport (Fig. 3B). This is due to differing pathways of warmer (less dense) water from colder (more dense) water. The majority of heat flux onto the shelf occurs through section AS1 and is primarily water that has recently entered the Bering Sea via eastern Aleutian Island Passes and is relatively warm. Differences between volume and heat flux are also due to the fact that exchanges between the ocean and atmosphere change the amount of heat in the ocean over time, while the volume remains relatively constant. The largest on-shelf oceanic heat flux is through Zhemchug Canyon (a total of 6.1 TW through sections AS4–AS6), with the second largest on-shelf heat flux through Bering Canyon (5.1 TW, section AS1). In Figs. 3B–D, several polygons are created by the cross-sections. We have summed the mean values of heat transport, salt flux, and freshwater flux across each section for each polygon, such that means directed into/outside the polygon are positive/negative. The resulting sum (the flux divergence) is shown circled and in italics inside each respective polygon. The flux divergence values shown in Fig. 3B indicate that a large amount of heat (2.5 TW) is lost to the atmosphere in the polygon northwest of Zhemchug Canyon, which is bounded by CS3, AS4, AS5, CS4, and AN4. Lower heat flux divergence values occur in the easternmost and westernmost polygons and also in the polygon north of the 50-m isobath.

A net loss of heat from the ocean to the atmosphere occurs as water generally moves northward throughout the Bering Sea toward the Chukchi Sea and Arctic Ocean. A total of 16.015 TW is advected onto the shelf across the 200-m isobath (Table 2). This calculation was made by summing the 26-year mean heat flux across the sections that lie along the 200-m isobath (AS1–AS9; shown in Figs. 2 and 3B). Approximately 75% of this heat is lost to the atmosphere between the 200- and 50-m isobaths. (The sections used in calculating the total heat flux across the

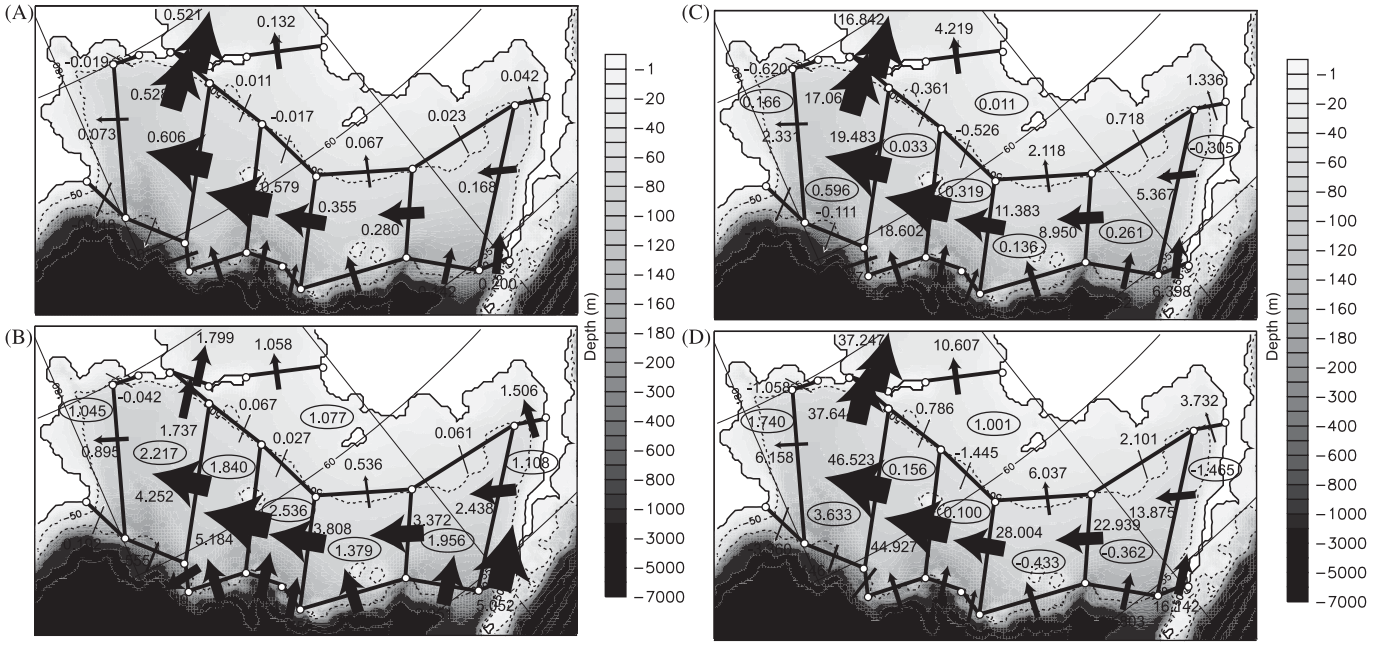

Fig. 3. Twenty-six-year (1979–2004) volume transport (Sv; A), heat flux (TW; relative to −0.1 °C; B), salt flux (million kg/s; C) and freshwater flux (mSv; relative to $S = 34.8$; D) across various sections. Arrows indicate net direction (positive is north or west) and are scaled relative to the largest value in each figure. The shading indicates depth (m). The 50 m and 200 m isobaths are shown as dotted lines. The mean flux divergence for each polygon is shown in italics and is circled.

50-m isobath were AN1–AN6.) A smaller loss occurs between the 50-m isobath and Anadyr and Shpanberg straits. Eventually, the net oceanic heat flux into the Chukchi Sea through Bering Strait is ~2.4 TW or 14.9% of the 200-m isobath value. This implies that an increase in Bering Sea heat content could have a large impact on the Arctic Ocean, especially in light of recent melting.

6. Salt and freshwater transport

The mean salt flux through the Bering Sea sections (Fig. 3C) closely resembles the mean volume transport in a relative sense, due to the strong dependence of salt flux on volume flux. Significant on-shelf salt fluxes occur between Bering Canyon and Zhemchug Canyon and, as a result, cross-shelf fluxes (CS1–CS5) on the outer shelf increase as the water moves northwestward across the shelf. The vast majority of salt transport on the outer shelf (17 million kg/s or 83% of the total) eventually crosses the 50-m isobath at AN6 near Anadyr Strait, with very little northward salt transport across the central and eastern sections. This is primarily due to bathymetric steering, as mentioned above in Section 4; the 50-m isobath directs the shelf flow toward AN6 and eventually northward through Anadyr Strait.

The mean freshwater flux (referenced to $S = 34.8$) through the Bering Sea sections shows that the primary freshwater route across the 200-m isobath is through the easternmost section (AS1). This section accounts for 31% of the total net northward freshwater transport along the 200-m isobath. Similar to volume and salt transport, the total freshwater flux accumulates as water moves northwestward across the shelf through sections CS1–CS5. Then, the majority of freshwater turns northeastward and flows through Anadyr Strait. Figs. 3C and D show that the polygon in the Gulf of Andyr (bounded by AN6, CS5, AS8, CS6, and AN7) has the highest values for salt and freshwater flux divergence. This is likely related to the large amount of sea ice produced and melted in this region, along with sea-ice export/import into the polygon from surrounding areas.

Table 2
Net heat transport (TW) across various locations in the Bering Sea.

Location	Heat transport (TW)	Percentage of 200-m isobath value
200-m isobath	16.015	N/A
50-m isobath	3.934	24.6
Anadyr+Shpanberg Straits	2.857	17.8
Bering Strait	2.383	14.9

7. Bering Slope Current and eddy kinetic energy

The BSC extends from the eastern Aleutian Islands along the shelf break toward Cape Navarin. It is a relatively broad, northwestward flow and, more recently, has been described as a system of eddies (Okkonen, 1993). Eddies ranging in size from 90 to 325 km are found to populate the Bering Sea basin, especially along the downstream portion of the BSC to the northwest. Several cross-sections across the BSC and across several canyons that lie along the Bering Sea shelf break were created to examine the flow and property fluxes in this region (locations of these cross-sections are shown in Fig. 4). Fig. 5 shows time series of monthly mean volume transport, heat flux, and section mean temperature through sections BSC1 and BSC4 from model results. The long-term mean volume transport for the BSC is 2–3.5 Sv. Flow reversals occur periodically at BSC1. However, at the westernmost section (BSC4), reversals occur multiple times per year, likely due to passing eddies. In fact, monthly mean volume transport at BSC4 ranges between −15 and 26 Sv.

The BSC carries a significant amount of heat (42–64 TW; Fig. 5), of which a portion is transported onto the shelf across the slope, as shown in Fig. 3B. Volume and heat transport are strongly correlated at BSC1 and BSC4 ($r = 0.99$ for monthly mean time series at each section). However, the low-frequency (smoothed) section mean temperature shows a different, somewhat decadal, signal. Section mean temperature was generally above average from 1979 to 1989 at BSC1 and BSC4. It then dropped below the 26-year mean from 1989 to 1998/1999 and has recently been above average. These temperature changes may be indirectly related to large-scale weather indices of the Arctic and/or North Pacific. However, no direct correlation exists between time series of monthly mean temperature at either BSC1 or BSC4 and any of the following climate indices: Arctic Oscillation (AO), Pacific Decadal Oscillation (PDO), and Pacific-North America Index (PNA). None of these correlations were significant at the 90% level and the absolute values of all correlation coefficients were <0.10.

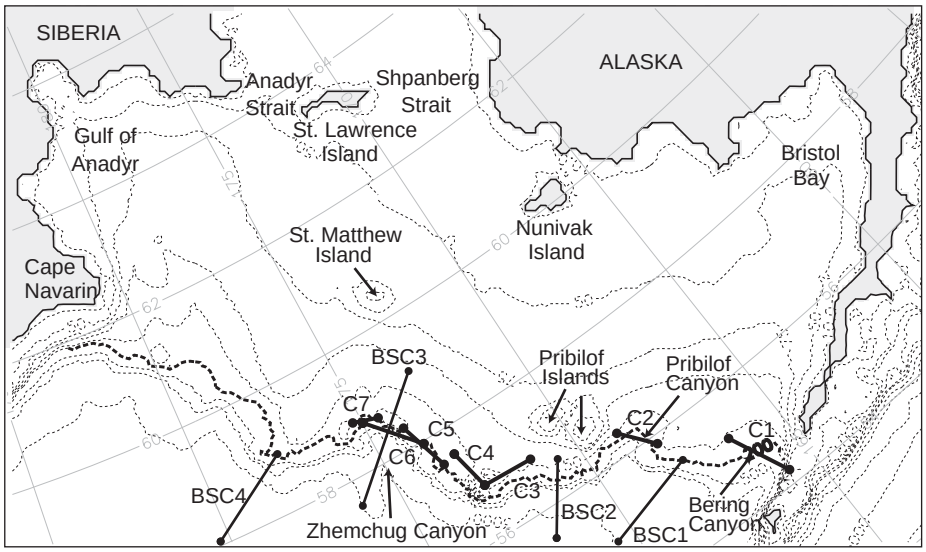

Fig. 4. Locations of Bering Slope Current and canyon cross-sections (solid black lines). The location of the 200-m isobath is shown as a thick dashed line.

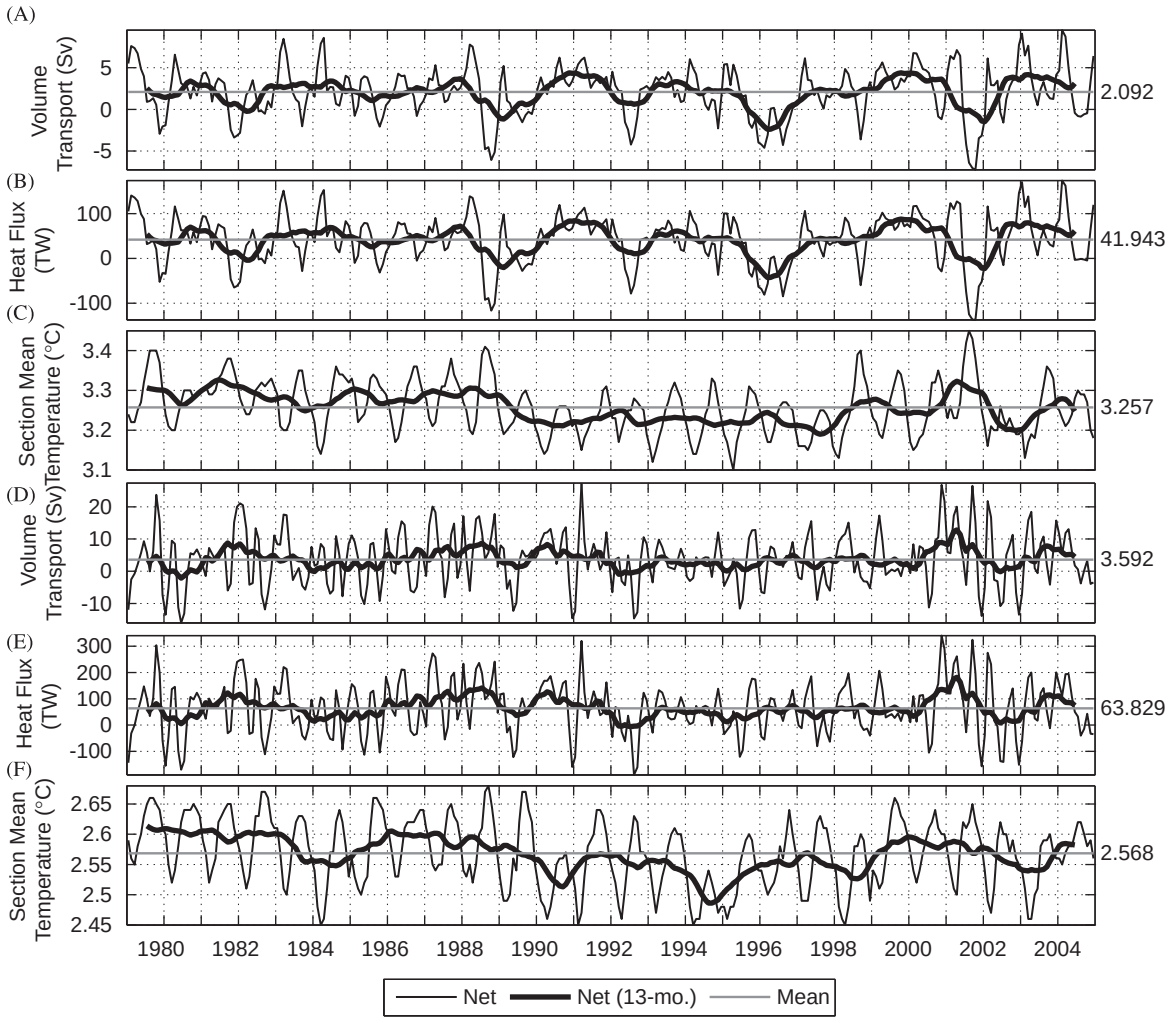

Fig. 5. Time series of monthly mean volume transport (A, D), heat flux (B, E), and mean temperature (C, F) across BSC1 (top three panels) and BSC4 (lower three panels). Heat flux is referenced to −0.1 °C. The thin black line represents monthly mean values, while the thick black line represents a 13-month running mean and the horizontal line represents the 26-year mean. Section locations are shown in Fig. 5.

Table 3
Correlation coefficients for volume transport, heat flux, and section mean temperature between Bering slope current sections.

Section 1	Section 2	Volume transport		Heat flux		Mean temperature	
		Mo. mean	Annual cycle removed	Mo. mean	Annual cycle removed	Mo. mean	Annual cycle removed
BSC1	BSC2	0.32 (0)	0.31 (4)	0.25 (0)	0.31 (4)	0.82 (0)	0.66 (0)
BSC1	BSC3	0.22 (0)	0.16 (0)	0.17 (0)	0.13 (0)	0.80 (0)	0.58 (0)
BSC1	BSC4	0.08 (0)	0.14 (7)	0.08 (0)	0.14 (7)	0.75 (0)	0.45 (0)
BSC2	BSC3	0.32 (0)	0.22 (0)	0.29 (0)	0.20 (0)	0.83 (0)	0.68 (0)
BSC2	BSC4	0.23 (1)	0.20 (1)	0.25 (0)	0.23 (1)	0.75 (0)	0.51 (0)
BSC3	BSC4	0.23 (5)	0.36 (5)	0.27 (5)	0.38 (5)	0.84 (0)	0.65 (0)

The number in parenthesis is the lag time in months. The first column (mo. mean) for each parameter is the correlation for the monthly mean values. The second column (annual cycle removed) is the correlation after removing the annual cycle.

Correlation coefficients for volume transport, heat flux, and mean temperature between the four BSC sections are shown in Table 3. We find a weak correlation for both volume transport and heat flux between BSC1 and BSC2, and these correlations become even less as fluxes across BSC1 are correlated with fluxes across sections further west. This is possibly due to the increased eddy activity in the west, which acts to reduce the correlation with the upstream portion of the current. Another possible explanation for the reduced correlation between time series at eastern and western sections is that sometimes the BSC separates from the shelf break. We have seen this separation in animations of sea surface height and also velocity throughout 26 years of model results. Over time scales of a few months, the position of the BSC is highly variable, especially in the western Bering Sea, and appears to be related to the formation of eddies just south of the shelf break. This separation from the shelf break is suggested in Figs. 1 and 2, where TKE is high (up to 100 $cm^2 s^{-2}$) near the junction of AS3–AS4 and near AS6–AS7. If the BSC separates from

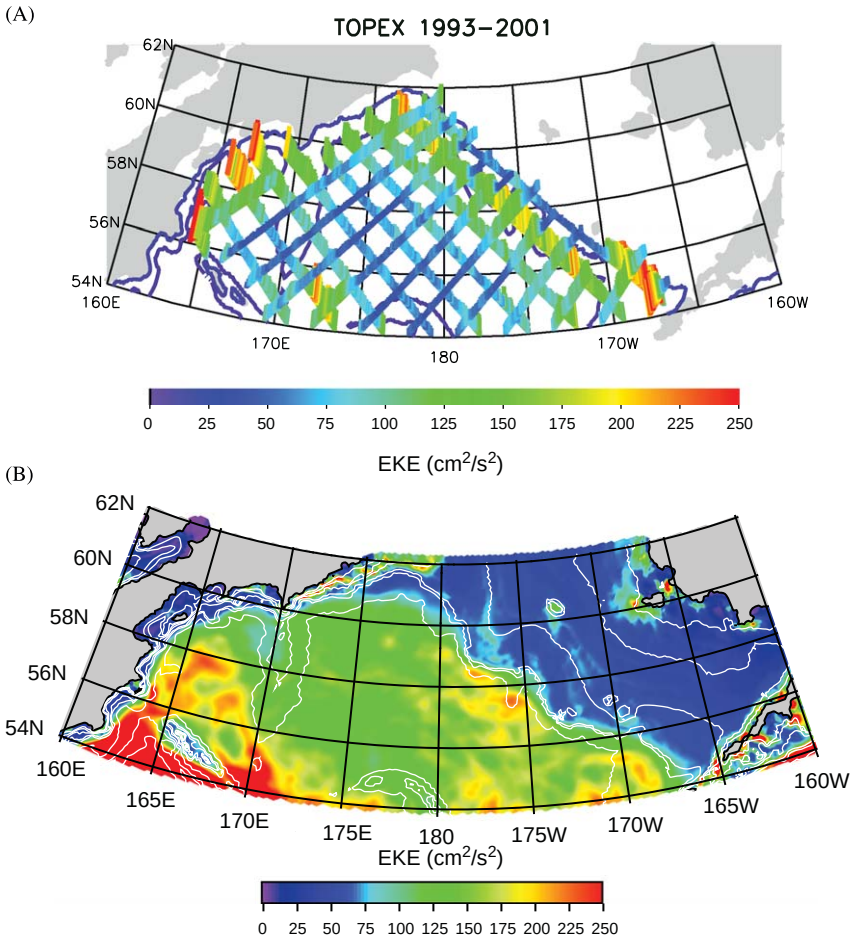

Fig. 6. Nine-year mean (1993–2001) eddy kinetic energy ($cm^2\,s^{-2}$) as computed from 10-daily fields from (A) TOPEX altimeter estimates of surface geostrophic velocity anomalies and (B) model surface velocities.

the shelf break, conditions at BSC4 are not likely to be similar to conditions at BSC1. Mean temperature is strongly correlated between all sections; however, it is important to note that there is no lag time. This, along with the lack of a strong correlation in volume transport, indicates that the temperature correlation is due to larger-scale basin changes in temperature, instead of an advected signal.

A previous study (Clement et al., 2005, Figs. 16 and 17) addressed the eddy kinetic energy (EKE) of the Bering Sea during 1987 utilizing model results from the same model described herein. Along the BSC, the EKE was 20–100 $cm^2\,s^{-2}$ southeast of Zhemchug Canyon, but was significantly higher (80–300 $cm^2\,s^{-2}$) northwest of Zhemchug Canyon. This is in agreement with Okkonen (1993), who found increased eddy activity in the downstream (western) leg of the BSC as compared to the upstream leg. However, it is possible that EKE is even higher in the real ocean, since our model is not yet fully eddy-resolving at 9-km horizontal resolution (Okkonen et al., 2007, Unpubl.).

In Fig. 6, we compare EKE from TOPEX altimeter measurements to model results. The TOPEX measurements show the regional distribution of EKE associated with surface geostrophic velocity anomalies computed from measurements of the sea surface height anomaly field. To approximate sampling associated with the 9.92-day TOPEX orbital repeat period, model EKE was computed from model surface velocities that were sub-sampled every 10 days. Both TOPEX measurements and model results depict the 9-year (1993–2001) mean of these 10-day fields. The TOPEX measurements are shown along orbital ground tracks with a vertical dimension that is proportional to EKE value (Fig. 6). TOPEX measurements are excluded (and not shown) on the shelf due to residual tidal contamination. The observed and modeled EKE show similar distributions; however, modeled values are somewhat higher than TOPEX values. In general, the TOPEX-derived estimates of EKE likely underestimate the true values. This is because altimeter-derived velocities are computed from the along-track slope of SSHA. Spatially, both the model and TOPEX show high EKE values along the shelf break and lower values in the basin interior. High values of EKE, up to 225 cm^2/s^2, are found near Zhemchug Canyon and along the southern part of the Kamchatka coast in both observations and model results.

8. Exchange in canyons and the importance of eddies

Figs. 3 and 6 indicate that transport, flux, and EKE measurements are locally enhanced near canyons along the Bering Sea slope: Bering Canyon, located on the north side of the Alaska Peninsula, Pribliof Canyon, located south of the Pribilof Islands, and Zhemchug Canyon, located along the shelf break in the central Bering Sea between 171°Wand 176°W (see Fig. 4 for canyon locations). Circulation and property exchange associated with these canyons is examined in greater detail below.

Twenty-six-year (1979–2004) mean values of volume, heat, salt, and freshwater transport through each canyon section are shown in Table 4. In the mean sense, the transport of water and all

properties is northward through all of the canyons. However, reversals do occur and may sometimes even show up at the monthly mean time scale (figures not shown). Because of the relatively strong on-shelf transports of volume, heat, and salt through section C6 (hereafter Zhemchug Canyon) we examine the relationship between conditions in the BSC and exchange through Zhemchug Canyon. Fig. 7 shows heat and salt flux anomalies through sections BSC3 and C6 (perpendicular sections whose locations are shown in Fig. 4). The two smoothed time series of heat flux anomaly are somewhat correlated, though not significantly at the 90% level ($r = 0.51$) with C6 lagging BSC3 by 4 months. The salt flux anomaly time series are slightly less correlated ($r = 0.44$), again with a 4-month lag and not significant at the 90% level. The salt flux anomaly is highly variable and peaks at over 10 million kg/s during November 1993 (indicated with an open circle in Fig. 7D). Based on Fig. 8C, we see that the increase in salt transported northward onto the shelf in November 1993 is associated with a cyclonic eddy located just south of the canyon section. The eddy has a diameter of 145 km and persists for a period of ~3 months. In addition, we show that three other peaks in the heat and salt flux anomalies are associated with cyclonic eddies (Fig. 8). These peaks are represented with stars on the time series in Figs. 7C and D. A vertical section along the Zhemchug Canyon (BSC3) during the maximum salt anomaly (November 1993) shows the high salinity anomaly core sitting above the slope, with positive salinity anomaly extending onto the shelf

Table 4
Twenty-six-year mean volume transport (Sv), salt flux (million kg/s), freshwater flux (mSv; relative to 34.8), and heat transport (TW; relative to −0.1 °C) for canyon sections.

Section	Volume transport	Salt flux	Freshwater flux	Heat flux
C1	0.206 (0.084)	6.601 (2.705)	15.842 (6.495)	5.245 (2.892)
C2	0.009 (0.080)	0.281 (2.579)	0.679 (6.120)	0.556 (1.505)
C3	0.083 (0.087)	2.682 (2.799)	6.198 (6.492)	1.261 (1.593)
C4	0.135 (0.053)	4.357 (1.717)	9.839 (3.840)	2.501 (1.233)
C5	0.110 (0.071)	3.556 (2.303)	7.895 (5.122)	2.035 (1.444)
C6	0.195 (0.112)	6.284 (3.616)	13.927 (7.976)	3.550 (2.369)
C7	0.055 (0.056)	1.782 (1.812)	3.960 (3.988)	1.004 (1.010)

Numbers in parenthesis represent standard deviation.

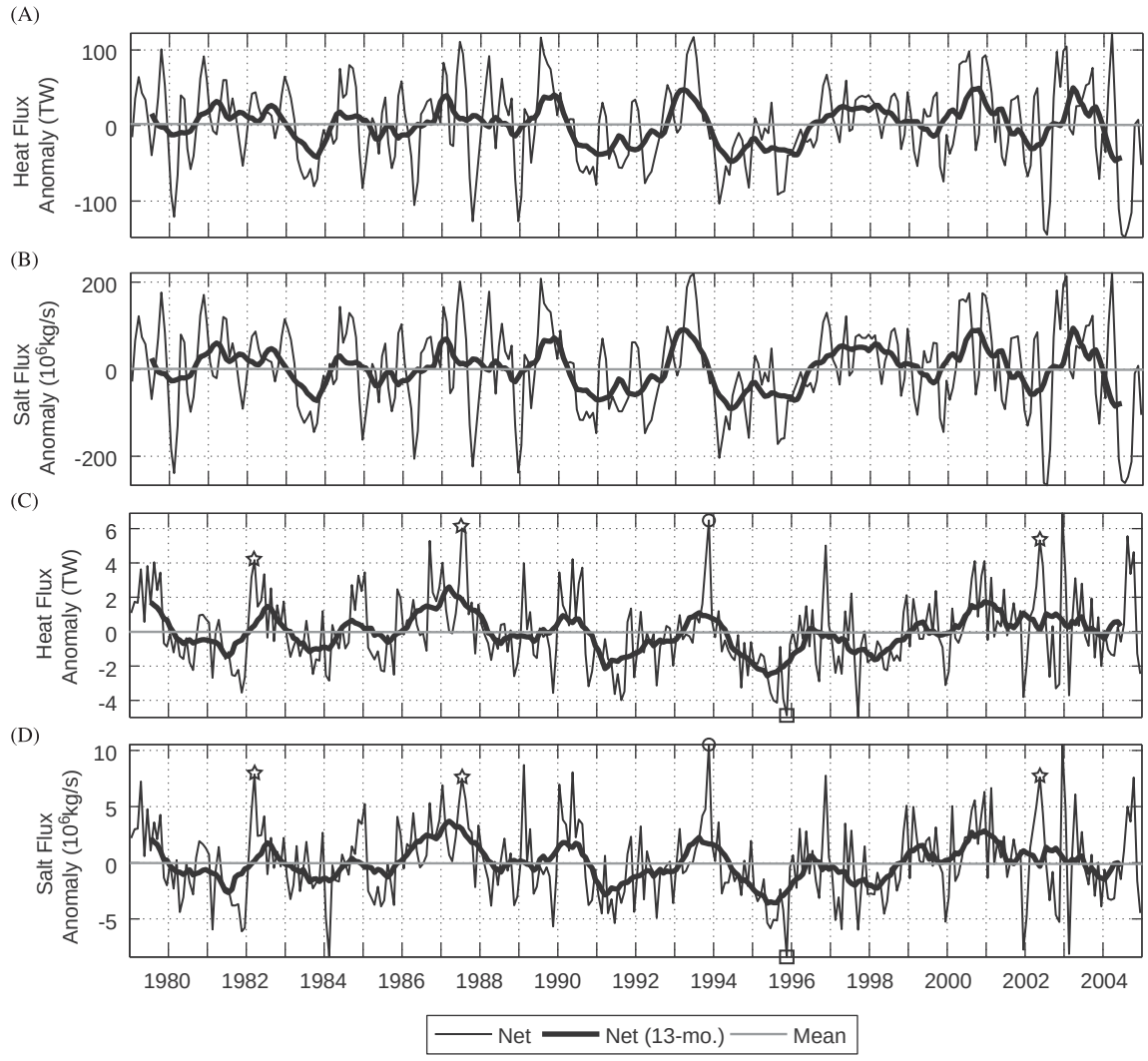

Fig. 7. Time series of monthly mean heat (A, C) salt (B, D) flux anomaly across BSC3 (A, B) and the Zhemchug Canyon section (C6; C, D) shown in Fig. 5. The thin black line represents monthly mean values, while the thick black line represents a 13-month running mean and the horizontal gray line represents zero. The circles and squares represent the salt and heat flux maximum (November 1993) and minimum (November 1995), respectively, through the Zhemchug Canyon. The stars represent local peaks in the heat and salt flux anomaly through the Zhemchug Canyon associated with eddies shown in Fig. 8.

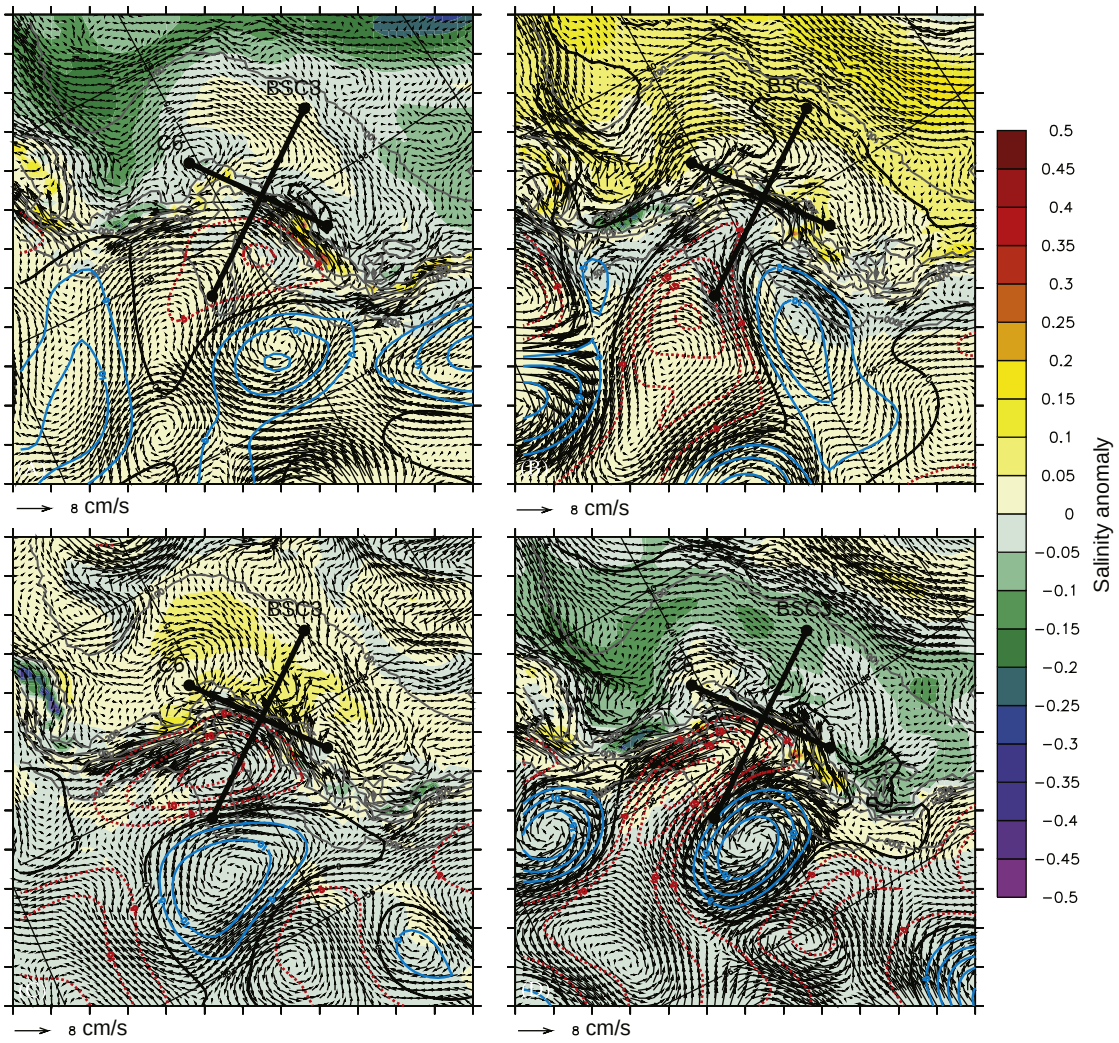

Fig. 8. Bottom-water salinity anomaly and sea surface height anomaly contours (blue is positive and red is negative; contour interval of 5 cm) during (A) March 1982, (B) July 1987, (C) November 1993, and (D) May 2002 in the vicinity of the Zhemchug Canyon. The vectors represent monthly mean velocity over the entire water column during each respective month.

(Fig. 9A). A section across Zhemchug Canyon (Fig. 9B) shows that the salinity anomaly is positive near the surface (up to 0.12 psu) and also near the bottom (up to 0.18 psu), with the flow directed on shelf. These figures show how the eddy is responsible for upwelling relatively salty water onto the central Bering Sea shelf. If we focus on the deeper water (>100 m, where salinity can be used as a proxy for nutrients), then we can say that this eddy accounted for a total of 28.6 trillion kg of salt being upwelled onto the shelf through the Zhemchug Canyon section during its 3-month lifetime. If we include the entire water column, then 107 trillion kg of salt were transported onto the shelf through Zhemchug Canyon during the same 3-month period.

The contribution of a transient motion (e.g., an eddy) to the time-averaged flux across a particular section can be quantified according to

$$\bar{F} = \int (\overline{uc})\,\mathrm{d}A \tag{1}$$

where $\bar{F}$ is a temporal mean flux (26-year annual cycle; 1979–2004), $\int(\ldots)\,\mathrm{d}A$ is the area integral across the section, u the normal component of velocity, and c the quantity being advected. We can define anomalies from the temporal mean

$$u' = u - \bar{u}, \quad c' = c - \bar{c} \tag{2}$$

Taking Eqs. (1) and (2) together gives

$$\bar{F} = \int (\bar{u}\bar{c})\,\mathrm{d}A + \int (\overline{u'c'})\,\mathrm{d}A \tag{3}$$

The perturbations, u' and c', should be derived from instantaneous measurements of u and c; or in the case of model results, calculated based on high-frequency temporal snapshot results. To make a fair calculation of the eddy transports, it would be best to use (for u and c) means that are daily, if not over a shorter time period. However, the model results are not available in three dimensions as daily means, due to storage limitations. Therefore, we must use the monthly means for calculating perturbation values. For the means ($\bar{u}$, $\bar{c}$) we use the 26-year annual cycle monthly means (e.g., mean January over 26 years). Transient motions contribute to the mean flux if u' and c' are correlated. The correlation coefficient between u' and S' across Zhemchug Canyon section was 0.32, while the correlation coefficient between u' and T' was 0.20. Both correlations were significant at the 99% level ($p = .01$). The fractional contribution of eddy transports to the mean flux, $\bar{F}$, was small for both heat and salt flux ($<8\%$). We argue that the weak correlations and small eddy contributions to the mean flux are largely due to the fact that we use monthly means for calculation of perturbation values, which smooth out the short-lived perturbations (Marble, 2001).

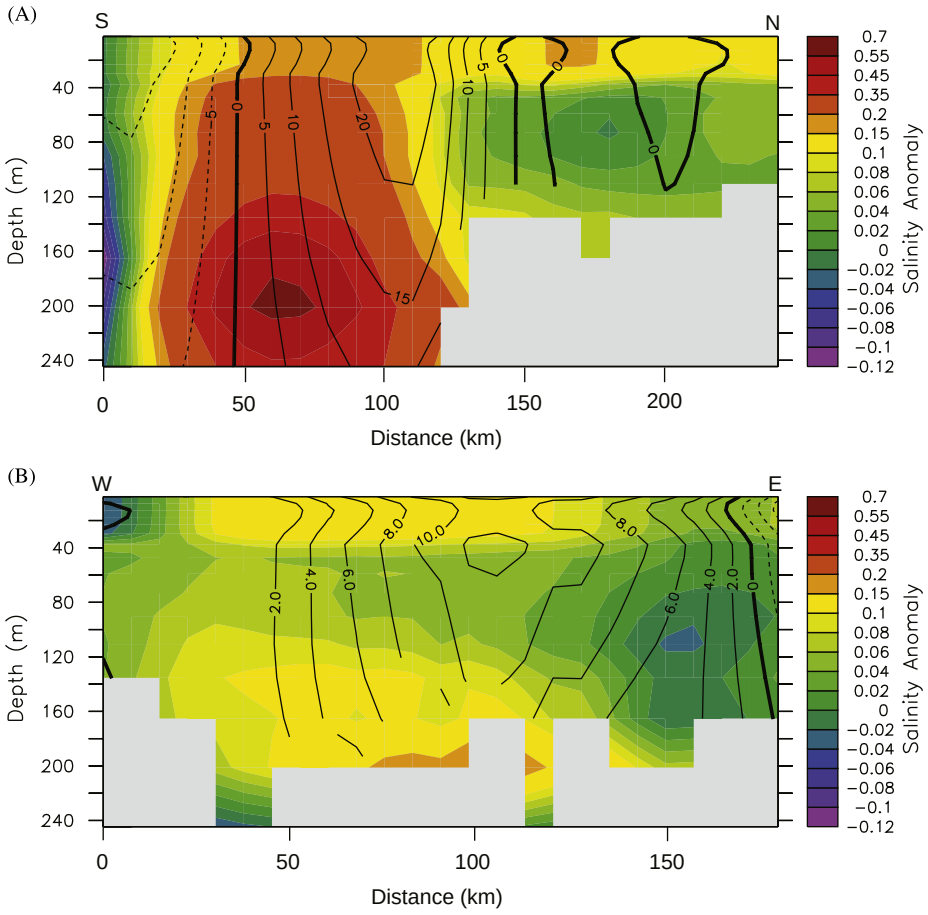

Fig. 9. Vertical section of velocity (contours; cm/s) and salinity anomaly (shading) (A) along the Zhemchug Canyon (section BSC3) and (B) across the Zhemchug Canyon (section C6) during November 1993.

We realize that this calculation does not fully quantify the eddy contribution to the mean flux; however, this is the best that can be made with the available model output.

Hovmuller plots of near-bottom salinity and temperature anomaly (after removing the annual cycle) for 1979–2004 allow us to see the significant interannual and spatial variability along the 200-m isobath (Fig. 10). Zhemchug Canyon experiences frequent events, likely due to strong eddy activity, in comparison to Bering Canyon, which is more consistent. Overall, we see that temperature and salinity anomalies tend to be of the same sign (either negative or positive) along the entire length of the 200-m isobath. However, this is not always true. For instance during 1987, temperature and salinity anomalies were negative in the west (0–400 km), with mainly positive anomalies in the east. When looking over longer time scales, we see that temperatures were higher, especially in the west during the 1980s, followed by a drop in the early 1990s. Recently, however, temperatures along the slope have increased. Salinity anomalies show some temporal similarities with temperature anomalies. Decreased salinity anomalies were present over the slope during the 1990s and increased in 2001. However, unlike temperature anomalies, the salinity was relatively low in the 1980s. There is also a suggestion of propagating features in these figures, possibly planetary waves, which would be a topic for a subsequent paper.

9. Discussion

The flow across the Bering Sea shelf is up to 3 cm/s in the mean sense and is the highest near 60°N between St. Matthew and Nunivak Islands. This area of strengthened flow is centered on and follows isobaths between 50 and 75 m. As expected, the strongest flow on the shelf is Anadyr Current to the west, which carries water toward Anadyr Strait at a mean speed of approximately 3–10 cm/s, depending on the location. Several regions along the slope (especially certain canyons) that are important in shelf–basin exchange also show up in the long-term mean circulation scheme (Fig. 1).

In our model results, the BSC appears to be more a system of eddies rather than a continuous current, which emphasizes the need for a fully eddy-resolving, basin-wide model to represent its complex dynamics. Okkonen (1993) identified a representative eddy period as ~4 months. This time period is similar to those of modeled high-frequency signals in the volume transport and heat flux at BSC4 (Figs. 5D and E), as well as the heat and salt flux anomalies at BSC3 (Fig. 7). The lack of correlation between various sections along the BSC, along with snapshots of SSH indicating frequent, multiple eddies (not shown), provide additional evidence for this conclusion.

We find little evidence for a north–south splitting of the BSC near Cape Navarin (Fig. 1). Instead the majority of the BSC turns southwestward on nearing the coast in the long-term mean model results. There is also evidence of a coastal current flowing northeastward around Cape Navarin. According to our model results the main source of water for the Gulf of Anadyr comes from the outer shelf flow, roughly between the 100- and 200-m isobaths.

Paluszkiewicz and Niebauer (1984) and Okkonen (1993) have suggested that topographic planetary waves generate eddies seen along the Bering slope. The modeled eddy described herein had a

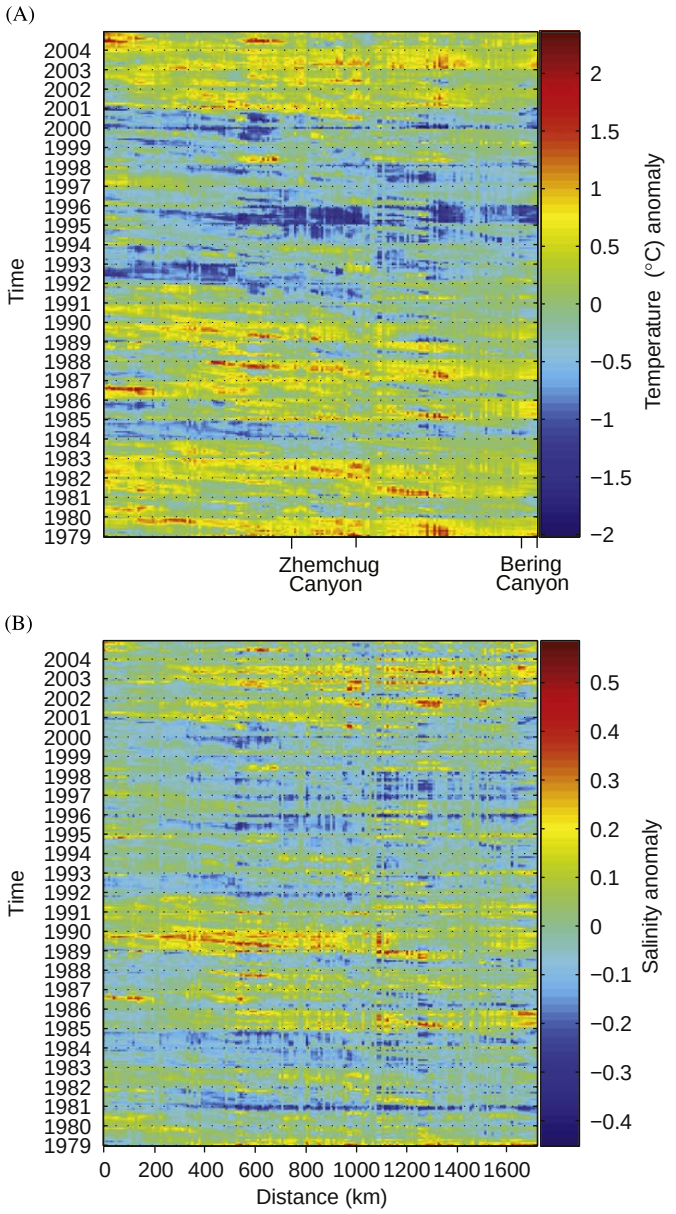

Fig. 10. Hovmuller plot of temperature anomaly (°C; A) and salinity anomaly (B) along the Bering Sea 200-m isobath.

diameter of 145 km and lifetime of ~90 days. This is similar in size and duration to eddies observed by Paluszkiewicz and Niebauer (1984; 140 km/84 days) and Okkonen (1993; 184 km/72 days). We conclude that frequent eddies, such as the one described herein, may be important for transporting salt onto the Bering Sea shelf. However, if we had been able to use three-dimensional daily mean fields to correlate velocity and salinity along the Zhemchug Canyon section, instead of monthly means, this might have allowed us to make a more quantitative statement. EKE and on-shelf transport appear to be enhanced by the presence of canyons along the Bering Sea slope (Figs. 3A, 6).

A biological 'hotspot' has been identified southwest of St. Lawrence Island between the 40- and 70-m isobaths (Grebmeier and Cooper, 1995). Our results show that a relatively strong source of on-shelf transport occurs south of this 'hotspot' in the Zhemchug Canyon region. Upwelling of nutrient-rich deep Bering Sea water due to eddies and shelf-basin exchange in general could enhance biological productivity in this region. For example, the eddy mentioned above in Section 8 had a mean salinity of 33.12, which can be converted to a silica concentration of 41.98 μM (based on a relation from data in Cooper et al., 1997). If we use the 3-month (October–December 1993) mean volume transport of 0.416 Sv, this yields a total of 8350 kg of silica advected onto the Bering Sea shelf through Zhemchug Canyon due to the eddy. If we focus on upwelled water (deeper than 100 m), the mean salinity is 33.36, which would be associated with a silica concentration of 45.61 μM. Over the 3-month lifetime of the eddy, the mean volume transport (for water deeper than 100 m) is 0.11 Sv, which would result in 2426 kg silica advected onto the Bering Sea shelf. It is important to note that this relationship between salinity and silica is a rough estimate. However, to our knowledge this is the first calculation of the amount of silica provided to the shelf via an eddy along the Bering Sea slope.

Acknowledgements

We thank the US National Science Foundation/Shelf–Basin Interactions (SBI) Program for primary support of this research. Additional support has been provided through other National Science Foundation Office of Polar Program (OPP) grants, the US Department of Energy Climate Change Prediction Program (CCPP), and the National Aeronautics and Space Administration Ocean and Ice Program. Computer resources were provided by the Arctic Region Supercomputing Center (ARSC) through the US Department of Defense High Performance Computer Modernization Program (HPCMP). Support for S. Okkonen was provided by the Cooperative Institute for Arctic Research of the University of Alaska. We thank Rodger Harvey, a guest editor of this volume, and two anonymous reviewers for insightful comments, which improved an earlier version of this manuscript.

References

Blumberg, A.F., Mellor, G.L., 1987. A description of a three-dimensional coastal ocean circulation model. In: Heaps, N. (Ed.), Three-Dimensional Coastal Ocean Models. American Geophysical Union, Washington, DC, pp. 1–16.

Busby, M.S., Mier, K.L., Brodeur, R.D., 2005. Habitat associations of demersal fishes and crabs in the Pribilof Island region of the Bering Sea. Fisheries Research 75, 15–28.

Chelton, D.B., deSzoeke, R.A., Schlax, M.G., Naggar, K.E., Siwertz, N., 1998. Geographical variability of the first baroclinic Rossby radius of deformation. Journal of Physical Oceanography 28, 433–460.

Ciannelli, L., Bailey, K.M., 2005. Landscape dynamics and resulting species interactions: the cod–capelin system in the southeastern Bering Sea. Marine Ecology Progress Series 291, 227–236.

Clement, J.L., Maslowski, W., Cooper, L., Grebmeier, J., Walczowski, W., 2005. Ocean circulation and exchanges through the northern Bering Sea—1979–2001 model results. Deep-Sea Research II 52, 3509–3540.

Codispoti, L.A., Flagg, C., Kelly, V., Swift, J.H., 2005. Hydrographic conditions during the 2002 SBI process experiments. Deep-Sea Reasearch II 52 (24–26), 3199–3226.

Cooper, L.W., Whitledge, T.E., Grebmeier, J.M., Weingartner, T., 1997. The nutrient, salinity, and stable oxygen isotope composition of Bering and Chukchi Seas waters in and near the Bering Strait. Journal of Geophysical Research 102, 12563–12573.

Grebmeier, J.M., Cooper, L.W., 1995. Influence of the St. Lawrence Island Polynya upon the Bering Sea benthos. Journal of Geophysical Research 100 (C3), 4439–4460.

Jakobsson, M., Cherkis, N., Woodward, J., Macnab, R., Coakley, B., 2000. New grid of Arctic bathymetry aids scientists and mapmakers. EOS Transactions of the AGU 81 (9), 89.

Kinder, T.H., Chapman, D.C., Whitehead, J.A., 1986. Westward intensification of the mean circulation on the Bering Sea shelf. Journal of Physical Oceanography 16, 1217–1229.

Marble, D.C., 2001. Simulated annual and seasonal Arctic Ocean and sea-ice variability from a high resolution, coupled ice–ocean model. Ph.D. Dissertation, Naval Postgraduate School, Monterey, CA.

Maslowski, W., Lipscomb, W.H., 2003. High-resolution simulations of Arctic sea ice during 1979–1993. Polar Research 22, 67–74.

Maslowski, W., Marble, D., Walczowski, W., Schauer, U., Clement, J.L., Semtner, A.J., 2004. On climatological mass, heat, and salt transports through the Barents Sea and Fram Strait from a pan-Arctic coupled ice–ocean model simulation. Journal of Geophysical Research 109, C03032.

Mizobata, K., Wang, J., Saitoh, S.I., 2006. Eddy-induced cross-slope exchange maintaining summer high productivity of the Bering Sea shelf break. Journal of Geophysical Research 111, C10017.

Mueter, F.J., Ladd, C., Palmer, M.C., Norcross, B.L., 2006. Bottom-up and top-down controls of walleye Pollock (*Theragra chalcogramma*) on the Eastern Bering Sea shelf. Progress in Oceanography 68, 152–183.

Okkonen, S., 1993. Observations of topographic planetary waves in the Bering Slope Current using Geosat altimeter. Journal of Geophysical Research 98 (12), 22603–22613.

Overland, J.E., Roach, A.T., 1987. Northward flow in the Bering and Chukchi Seas. Journal of Geophysical Research 92, 7097–7105.

Overland, J.E., Spillane, M.C., Hurlburt, H.E., Wallcraft, A.J., 1994. A numerical study of the circulation of the Bering Sea basin and exchange with the North Pacific Ocean. Journal of Physical Oceanography 24, 736–758.

Paluszkiewicz, T., Niebauer, H.J., 1984. Satellite observations of circulation in the eastern Bering Sea. Journal of Geophysical Research 89, 3663–3678.

Royer, T.C., 1981. Baroclinic transport in the Gulf of Alaska, Part II. A fresh water driven Coastal Current. Journal of Marine Research 39, 251–266.

Shuert, P.G., Walsh, J.J., 1993. A coupled physical–biological model of the Bering–Chukchi Seas. Continental Shelf Research 13, 543–573.

Stabeno, P.J., Schumacher, J.D., Ohtani, K., 1999. The physical oceanography of the Bering Sea. In: Loughlin, T.R., Ohtani, K. (Eds.), Dynamics of the Bering Sea. University of Alaska Sea Grant, Fairbanks, AK, pp. 1–28.

Spaulding, M., Isaji, T., Mendelsohn, D., Turner, A.C., 1987. Numerical simulation of wind-driven flow through the Bering Strait. Journal of Physical Oceanography 17, 1799–1816.

Steele, M., Morley, R., Ermold, W., 2000. PHC: a global ocean hydrography with a high quality Arctic Ocean. Journal of Climate 14 (9), 2079–2087.

Walsh, J.J., McRoy, C.P., Coachman, L.K., Goering, J.J., Nihoul, J.J., Whitledge, T.E., Blackburn, T.H., Parker, P.L., Wirick, C.D., Shuert, P.G., Grebmeier, J.M., Springer, A.M., Tripp, R.D., Hansell, D.A., Djenidi, S., Deleersnijder, E., Henriksen, K., Lund, B.A., Andersen, P., Mülller-Karger, F.E., Dean, K., 1989. Carbon and nitrogen cycling within the Bering/Chukchi Seas: source regions for organic matter effecting AOU demands of the Arctic Ocean. Progress in Oceanography 22, 277–359.